Dielectrophoretic Manipulation of DNA: Separation and Polarizability

5 AUTHORS, INCLUDING:

Jan Regtmeier
Bielefeld University
27 PUBLICATIONS   **467** CITATIONS

SEE PROFILE

Dario Anselmetti
Bielefeld University
221 PUBLICATIONS   **5,133** CITATIONS

SEE PROFILE

Dielectrophoretic Manipulation of DNA: Separation and Polarizability

Jan Regtmeier,[†] Thanh Tu Duong,[†] Ralf Eichhorn,[‡] Dario Anselmetti,[†] and Alexandra Ros*,[†]

Experimental Biophysics and Applied Nanoscience and Condensed Matter Theory, Physics Department, Bielefeld University, Universitätsstrasse 25, 33615 Bielefeld, Germany

Although separation of polymers based on the combination of dielectrophoretic trapping and electrophoretic forces was proposed 15 years ago, experimental proof has not yet been reported. Here, we address this problem for long DNA fragments in a simple and easy-to-fabricate microfluidic device, in which the DNA is manipulated by electrophoresis and by electrodeless dielectrophoresis. By slowly increasing the strength of the dielectrophoretic traps in the course of the separation experiments, we are able to perform efficient and fast DNA separation according to length for two different DNA conformations: linear DNA (λ (48.5-kbp) and T2 (164-kbp) DNA) and supercoiled covalently closed circular plasmid DNA (7 and 14 kbp). The underlying migration mechanism—thermally induced escape processes out of the dielectrophoretic traps in the direction of the electrophoretic force—is sensitive to different DNA fragments because of length-dependent DNA polarizabilities. This is analyzed in a second series of experiments, where the migration mechanism is exploited for the quantitative measurement of the DNA polarizabilities. This new and simple technique allows for the systematic characterization of the polarizability not only for DNA but also for other biomolecules like proteins. Furthermore, our results have direct implications to future biotechnological applications such as gene therapy and DNA vaccination.

Manipulating biological objects like biomolecules by electric fields is crucial for implementing techniques for their transport, mixing, concentration, fractionation, or separation in microfluidic lab-on-a-chip systems. In developing such methods, the (quantitative) characterization of the particle behavior in the presence of electric fields is an important concomitant problem. These aspects are addressed in the present article for the dielectrophoresis of DNA: the technological application for separation, and the quantitative characterization of the relevant DNA property, namely, its polarizability. To this end, the dielectrophoretic manipulation of DNA by inhomogeneous electric fields due to polarization effects is combined with electrophoresis, where migration of the charged molecule in the electrolyte is induced by an electric field.

In order to induce dielectrophoresis, inhomogeneous electric fields are usually generated by microelectrodes.[1] Alternatively, inhomogeneous electric fields of high strength are also obtained without microelectrodes[2] (i.e., electrodeless) by the use of nonconducting posts in microfluidic channels,[3−5] thereby reducing the complexity of the fabrication processes involved and, more importantly, providing field gradients over the entire depth of the microchannel. Using such inhomogeneous fields, dielectrophoresis has proven to be applicable for the specific manipulation of particles,[6,7] cells,[8,9] and viruses[10] as well as biomolecules such as DNA[11] and even single proteins.[12] In particular, the dielectrophoretic manipulation of DNA has been increasingly studied over the last years, including the investigation of DNA dielectrophoresis in microfluidic devices.[4,13−15] For instance—and most relevant to the present study—electrodeless dielectrophoresis of single- and double-stranded DNA was thoroughly discussed by Chou et al.,[4] demonstrating size-dependent frequency response for DNA fragments from 368 bp to 39.9 kbp below 1 kHz. Similarly, frequency-dependent dielectrophoretic trapping of DNA using microelectrodes was reported in ref 14 for a frequency range below 1 kHz. However, the mechanisms involved in DNA polarization as well as the dependence of the dielectrophoretic response on the DNA length remain unclear.[16,17] The DNA polarizability strongly de-

(1) Hughes, M. P. *Electrophoresis* **2002**, *23*, 2569−82.
(2) Chou, C.-F.; Zenhausern, F. *IEEE Eng. Med. Biol. Mag.* **2003**, *22*, 62−7.
(3) Cummings, E. B.; Singh, A. K. *Anal. Chem.* **2003**, *75*, 4724−31.
(4) Chou, C.-F.; Tegenfeldt, J. O.; Bakajin, O.; Chan, S. S.; Cox, E. C.; Darton, N.; Duke, T.; Austin, R. H. *Biophys. J.* **2002**, *83*, 2170−9.
(5) Lapizco-Encinas, B. H.; Simmons, B. A.; Cummings, E. B.; Fitschenko, Y. *Anal. Chem.* **2004**, *76*, 1571−9.
(6) Gascoyne, P. R. C.; Vykoukal, J. V. *Electrophoresis* **2002**, *23*, 1973−83.
(7) Dürr, M.; Kentsch, J.; Müller, T.; Schnelle, T.; Stelzle, M. *Electrophoresis* **2003**, *24*, 722−31.
(8) Fiedler, S.; Shirley, S. G.; Schnelle, T.; Fuhr, G. *Anal. Chem.* **1998**, *70*, 1909−15.
(9) Huang, Y.; Joo, S.; Duhon, M.; Heller, M.; Wallace, B.; Xu, X. *Anal. Chem.* **2002**, *74*, 3362−71.
(10) Morgan, H.; Hughes, M. P.; Green, N. G. *Biophys. J.* **1999**, *77*, 516−25.
(11) Bakewell, D. J.; Morgan, H. *IEEE Trans. Nanobiosci.* **2006**, *5*, 1−8.
(12) Hölzel, R.; Calander, N.; Chiragwandi, Z.; Willander, M.; Bier, F. F. *Phys. Rev. Lett.* **2005**, *95*, 128102-1−128102-4.
(13) Lao, A. I. K.; Hsing, I.-M. *Lab Chip* **2005**, *5*, 687−90.
(14) Asbury, C. L.; Diercks, A. H.; van der Engh, G. *Electrophoresis* **2002**, *23*, 2658−66.
(15) Washizu, M.; Suzuki, S.; Kurosawa, O.; Nishizaka, T.; Shinohara, T. *IEEE Trans. Ind. Appl.* **1994**, *30*, 835−43.
(16) Bakewell, D. J.; Ermolina, I.; Morgan, H.; Milner, J.; Feldman, Y. *Biochim. Biophys. Acta* **2000**, *1493*, 151−8.
(17) Porschke, D. *Biophys. Chem.* **1997**, *66*, 241−57.

* Corresponding author. E-mail: Alexandra.Ros@physik.uni-bielefeld.de.
† Experimental Biophysics and Applied Nanoscience.
‡ Condensed Matter Theory.

pends on the frequency range and buffer conditions (e.g., ionic strength) used and is quantitatively accessible usually in bulk measurements by birefringence,[18-20] conductivity dispersion,[21] or time domain reflectometry.[16]

The field of DNA separation technologies is governed by the fact that the free electrophoretic mobility of DNA fragments is independent of the fragment length. To nevertheless obtain length-dependent migration behavior, gel-based electrophoretic separation methods are most commonly used, where pulsed field conditions are usually employed for long DNA fragments (>40 kbp). The latter method has its drawback in long separation times with duration from 10 h up to 200 h. Several alternative approaches for DNA separation in "gel-free" media using microfluidic devices have been proposed over the last years. Successful and efficient separation of DNA fragments of >40 kbp has been demonstrated in micro-[22-25] and nanopillar[26] arrays as well as in magnetic bead[27,28] or nanosphere matrices.[29] Size-dependent migration and efficient separation have been performed in periodically structured microfluidic channels[30,31] and by using entropic traps.[32-34] Ratchet effects in asymmetric periodic microstructures have been shown to induce directed transport[35,36] and continuous-flow separation of DNA.[37] In contrast, the combination of dielectrophoresis with free-flow electrophoresis for the separation of DNA molecules with length-dependent polarizabilities, as suggested theoretically by Ajdari and Prost,[38] has not been realized experimentally yet.

In this paper, we demonstrate the proof of concept for DNA separation based on dielectrophoretic trapping in high-field regions. In a structured microfluidic device that consists of an array of insulating posts, linear as well as circular covalently closed (ccc) DNA samples in a size range between 7 and 164 kbp are separated within separation times of a few minutes with baseline resolution. Furthermore, based on a theoretical analysis of the
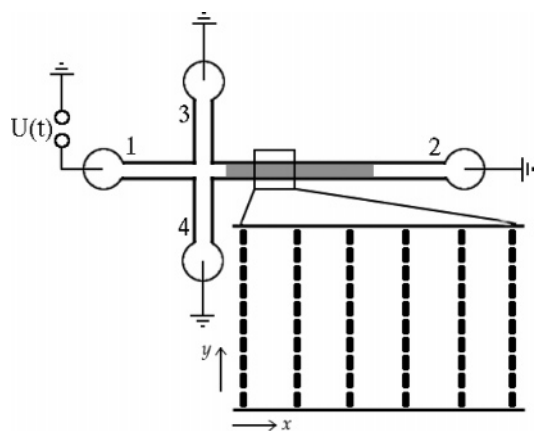

Figure 1. Scheme of the microfluidic setup (not to scale). The microfluidic device is composed of four linear channels forming a cross with four fluid reservoirs at their ends. The channels 1, 3, and 4 (each of length 2 mm) serve for fluid access and injection (cross injector); channel 2 (length 5 mm) contains the microstructure (indicated by the gray region) in which dielectrophoretic trapping and separation is performed. The channel depth in the whole device is 6 μm; the channel width is 100 μm for channels 1 and 2 and 95 μm for channels 3 and 4. As illustrated with the enlargement, the microstructure in channel 2 consists of periodically arranged rows of rectangular posts (180 rows) with a period L = 21.1 μm along the channel axis (x direction) and a distance 2.3 μm between posts in the direction perpendicular to the channel axis (y direction); the size of the posts in the $x-y$ plane is 2.2 × 7.4 μm². After the DNA is injected into channel 2 by a pinched injection scheme, the driving voltages $U(t)$ for dielectrophoretic DNA manipulation in the microstructure are applied in reservoir 1, whereas all other reservoirs are grounded.

size-dependent DNA migration behavior in the dielectrophoretic energy landscape, we develop a novel method for the quantitative deduction of the DNA polarizability; the results for four linear DNA fragment sizes indicate a power law dependence of their polarizability on chain length with an exponent comparable to the Flory exponent.

MATERIALS AND METHODS

Chemicals. Si wafers (5 in.) were purchased from CrysTec. The negative photoresist SU-8 was obtained from Microresist. Sylgard 184, composed of the base polymer and the curing agent for poly(dimethylsiloxane) (PDMS), was purchased from Spoerle Elektronik. Plasmid DNA (7 and 14 kbp) was a generous gift from PlasmidFactory (Bielefeld, Germany). T2-DNA, disodium hydrogen phosphate dihydrate, NaCl, EDTA, and 2-mercaptoethanol were purchased from Fluka, λ-DNA was from Promega, and linear 6- and 12-kbp DNA was from MBBL. Glass slides were obtained from Menzel-Gläser, and Pt wire (0.4-mm diameter) was from VWR. Deionized water was supplied by a Milli-Q Biocel (Millipore). YOYO-1 for DNA staining was purchased from Molecular Probes . The bifunctional poly(ethylene glycol) (PEG) silane SIL-3400 (PEG chain length 70) was obtained from Nektar, tridecafluoro-1,1,2,2-tetrahydrooctyltrichlorosilane from ABCR, and performance-optimized polymer 6% (POP-6) from Applied Biosystems.

Fabrication of the Structured Microfluidic Chip. The microfluidic device (see Figure 1) was fabricated from PDMS by soft lithography as reported in ref 31. Briefly, the inverted relief of the microstructure was created on a Si wafer using contact photolithography of SU-8 with a predesigned photomask. PDMS

(18) Stellwagen, N. C. *Biopolymers* **1981**, *20*, 399−434.
(19) Elias, J. G.; Eden, D. *Macromolecules* **1981**, *14*, 410−9.
(20) Rau, D. C.; Bloomfield, V. A. *Biopolymers* **1979**, *18*, 2783−805.
(21) Hanss, M.; Bernengo, J. C. *Biopolymers* **1973**, *12*, 2151−9.
(22) Inatomi, K.; Izuo, S.; Lee, S.; Ohji, H.; Shiono, S. *Microelectr. Eng.* **2003**, *70*, 13−8.
(23) Bakajin, O.; Duke, T. A. J.; Tegenfeldt, J.; Chou, C. F.; Chan, S. S.; Austin, R. H.; Cox, E. C. *Anal. Chem.* **2001**, *73*, 6053−6.
(24) Huang, L. R.; Tegenfeldt, J. O.; Kraeft, J. J.; Sturm, J. C.; Austin, R. H.; Cox, E. C. *Nat. Biotechnol.* **2002**, *20*, 1048−51.
(25) Huang, L. R.; Cox, E. C.; Austin, R. H.; Sturm, J. C. *Science* **2004**, *304*, 987−90.
(26) Kaji, N.; Tezuka, Y.; Takamura, Y.; Ueda, M.; Nishimoto, T.; Nakanishi, H.; Horiike, Y.; Baba, Y. *Anal. Chem.* **2004**, *76*, 15−22.
(27) Doyle, P. S.; Bibette, J.; Bancaud, A.; Viovy, J.-L. *Science* **2002**, *295*, 2237.
(28) Minc, N.; Fütterer, C.; Dorfman, K. D.; Bancaud, A.; Gosse, C.; Goubault, C.; Viovy, J.-L. *Anal. Chem.* **2004**, *76*, 3770−6.
(29) Tabuchi, M.; Ueda, M.; Kaji, N.; Yamasaki, Y.; Nagasaki, Y.; Yoshikawa, K.; Kataoka, K.; Baba, Y. *Nat. Biotechnol.* **2004**, *22*, 337−40.
(30) Ros, A.; Hellmich, W.; Duong, T.; Anselmetti, D. *J. Biotechnol.* **2004**, *122*, 65−72.
(31) Duong, T.; Kim, G.; Ros, R.; Streek, M.; Schmid, F.; Brugger, J.; Ros, A.; Anselmetti, D. *Microelectr. Eng.* **2003**, *67−68*, 905−12.
(32) Han, J.; Craighead, H. G. *Anal. Chem.* **2002**, *74*, 394−401.
(33) Han, J.; Craighead, H. G. *Science* **2000**, *288*, 1026−9.
(34) Fu, J.; Yoo, J.; Han, J. *Phys. Rev. Lett.* **2006**, *97*, 018103-1-4.
(35) Bader, J. S.; Hammond, R. W.; Henck, S. A.; Deem, M. W.; McDermott, G. A.; Bustillo, J. M.; Simpson, J. W.; Mulhern, G. T.; Rothberg, J. M. *Proc. Natl. Acad. Sci. U.S.A.* **1999**, *96*, 13165−9.
(36) Hammond, R. W.; Bader, J. S.; Henck, S. A.; Deem, M. W.; McDermott, G. A.; Bustillo, J. M.; Rothberg, J. M. *Electrophoresis* **2000**, *21*, 74−80.
(37) Huang, L.; Cox, E.; Austin, R. H.; Sturm, J. C. *Anal. Chem.* **2003**, *75*, 6963−7.
(38) Ajdari, A.; Prost, J. *Proc. Natl. Acad. Sci. U.S.A.* **1991**, *88*, 4468−71.

was cast on that master wafer, and after curing for 4 h at 85 °C, the structured PDMS slab was carefully peeled off. Reservoir holes of 2-mm diameter were punched through the PDMS at the ends of the channels; their position was determined using a modified microscope with a nonius, providing an alignment precision of ~±100 μm.

The structured PDMS slab and a glass slide with a thin spin-coated layer of PDMS were then cleaned in acetone, ethanol and deionized water in an ultrasonic bath. The glass slide and the structured PDMS slab were oxidized in a home-built oxygen plasma chamber for 30 s (50 kV, 500 kHz, 0.1 mbar oxygen, distance of electrodes 6.2 cm).[39] Both oxidized surfaces were brought into contact immediately after the treatment, forming an irreversible seal.

For easy handling and good reproducibility, a poly(methyl methacrylate) (PMMA) block ($56 \times 80 \times 5$ mm^3) was used on top of the PDMS device to enlarge the reservoirs of the chip and to hold the chip and the Pt electrodes in place. To that end, reservoir access holes with a diameter of 2 mm were drilled through the PMMA block at the corresponding positions. Additionally, diagonal holes were drilled at an angle of 45° for the Pt electrodes, which were fixed with a two-component epoxy resin. Before each experiment, the PMMA block was rinsed with DI water, dried, and subsequently pressed manually onto the PDMS chip. The chip adhered to the PMMA reversibly, but without leakage.

Microfluidic Operations. A PEG coating of the inner channel walls was performed by flushing a solution of ~3 μM SIL-3400 for 15 min through all microfluidic channels.[39] The device was subsequently filled with 10 mM phosphate solution (pH 8.3, 2 mM NaCl, 1 mM EDTA, 0.2% (v/v) 2-mercaptoethanol, 0.1% POP-6). DNA samples were prepared with ~1 YOYO-1 molecule/10 base pairs.

For the separation experiments and DNA velocity measurements, the cross-injector (see Figure 1) delivered defined sample volumes (~60 fL) of DNA molecules by a pinched injection protocol into the structured separation channel (channel 2 in Figure 1), as previously reported.[30] After injection, the driving voltages were switched to a sinusoidal ac voltage $U(t) = U_{ac} \sin(\omega t)$ to create a dielectrophoretic potential landscape, superimposed by a static component U_{dc} to induce directed motion of the DNA by electrophoresis. These voltages were applied at the device electrodes as indicated in Figure 1.

Voltage Control and Detection. The sinusoidal voltage signal was created via a LabView 6i program and a DAQ card 6036E (National Instruments). The output signal with a maximum amplitude of 10 V was amplified by a high-voltage amplifier (600H, NanoTechTools) and applied to the Pt electrodes via Micro-Kleps (Conrad Elektronik GmbH). For the DNA separation experiments (Figure 3), a protocol employing an U_{ac} ramp was applied: starting from an initial voltage U_{start}, the value of U_{ac} was increased every τ seconds by a voltage step U_{inc} until the final voltage U_{end} was reached. Immediately after reaching U_{end}, the U_{ac} voltage was set to the maximal value $U_{max} = 420$ V in order to permanently trap the DNA, which is necessary for recording a steady-state electropherogram of the separated DNA. The explicit values of U_{start},
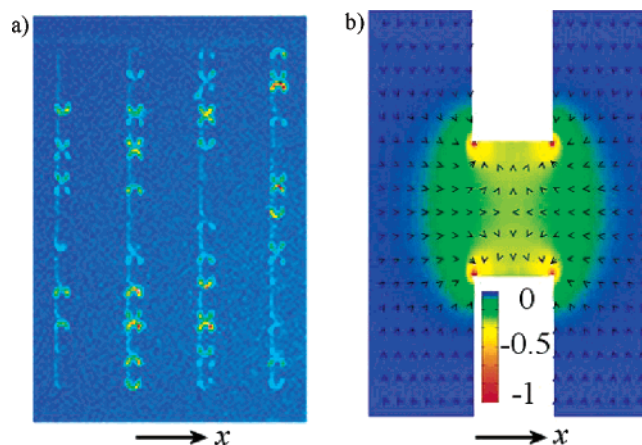

Figure 2. (a) Fluorescence micrograph of fluorescently stained T2-DNA that is trapped by dielectrophoresis in the high-field regions in the gaps between neighboring posts ($U_{ac} = 300$ V, $\omega = 60$ Hz). (b) Dielectrophoretic potential $W = -(1/2)\alpha E^2$ (see eq 1) in a gap between two posts (white rectangles) in the case of positive dielectrophoresis ($\alpha > 0$). The electric field is numerically calculated as described in Materials and Methods. The color code indicates the magnitude of the potential energy in arbitrary units. The arrows indicate direction of the resulting dielectrophoretic force field. Potential minima occur near the edges of the posts.

U_{end}, U_{inc}, and τ for each separation experiment are given in the corresponding caption of Figure 3.

An inverted light microscope (Axiovert 200, Zeiss) with a motorized x/y-stage (99S008, Ludl Electronic Products), a 100× oil immersion objective (Plan Neofluar, NA 1.3, Zeiss), a mercury arc lamp (HBO 100) for excitation of stained DNA molecules, a gray filter (transmittance 25%) for reduction of incident light intensity, and a fluorescence filter set (BP 450-490, FT 510, BP 515-565, Zeiss) were used for single DNA molecule observation. A CCD interline-transfer camera (Imager3LS, LaVision) with corresponding grabber card and software (DaVis 6.2) was used for data acquisition. Video sequences of the DNA motion in the microfluidic channel were recorded at 10 frames/s. From these video sequences, DNA velocities were determined by single-molecule tracking. The locations of dielectrophoretically trapped (and thus immobile) DNA were determined by setting the x/y stage to automatic translation along the axis of the structured channel (x direction) with a constant velocity of 10 μm/s toward the cross-injector and recording the fluorescence signal of the DNA at a frame rate of 3 frames/s. These images were transformed into a plot of the fluorescence intensity as a function of the position x in the channel using a script written in DaVis own CL language. In the context of the separation experiments we call such plots steady-state electropherograms.

Calculation of the Electric Field. To calculate the electric field $\vec{E}$, we numerically solved the Laplace equation in a region that comprises several spatial periods of the microstructure in x and y directions, with the following boundary conditions (see also ref 40): a preset potential difference along the x axis (representing a static voltage applied to the device; see Figure 1), periodic in y direction (reflecting the periodicity of the microstructure), and Neumann boundary conditions at the borders between buffer

(39) Hellmich, W.; Regtmeier, J.; Duong, T.; Ros, R.; Anselmetti, D.; Ros, A. *Langmuir* **2005**, *21*, 7551−7.

(40) Ros, A.; Eichhorn, R.; Regtmeier, J.; Duong, T. T.; Reimann, P.; Anselmetti, D. *Nature* **2005**, *436*, 928.

solution and microstructure. The latter are a consequence of the assumption that the buffer is a perfect electric conductor, whereas the microstructure material PDMS is a perfect insulator. The solution of the Laplace equation is computed with a program that uses the Laplace solver D03EAF of the numerical algorithms group[41] library.

The specific potential drop at the post array that results from the voltage U, when applied to the device electrodes as shown in Figure 1, can be quantitatively obtained as follows. Since the fluid is an ideal conductor, we can interpret the microfluidic channels as an electric circuit.[42] Each segment of the microfluidic channels with constant fluid-occupied cross-sectional area can be represented by a resistor that is proportional to the segment length and inversely proportional to that area. The proportionality factor (electrical resistivity) is of no interest, since only ratios of resistances are needed in the present calculation. Applying Kirchhoff's laws to the resulting circuit diagram, one can determine the fraction of the applied voltage U that acts at a row of posts as well as the voltage drop between two successive rows of posts from the geometrical properties of the microdevice. Using the numbers given with Figure 1, we obtain that the voltage drop at a row of posts is $4.9 \times 10^{-4} U$.

Finally, the average electric field amplitude E_{gap} in the gaps between the posts is estimated by dividing this potential drop by the size of the gaps in field direction (which is 2.2 μm) with the result $E_{gap} \approx 220U\,m^{-1}$. For comparison, a simple estimate of the electric field by assuming that the voltage U is applied over the total length of the channels 1 and 2 would yield a factor 140 instead of 220.

RESULTS AND DISCUSSION

Dielectrophoretic Trapping. We first verify that the microfluidic device of Figure 1 is suitable for dielectrophoretic manipulation of long DNA fragments. In Figure 2a, the typical experimental situation is shown for T2 (164 kbp) DNA in the microstructure that is subjected to a time-dependent voltage $U(t) = U_{ac}\sin(\omega t)$ with frequency $\omega = 60$ Hz and amplitude $U_{ac} = 300$ V. The DNA is permanently (i.e., within our observation time) trapped within the gaps close to the post walls, very similar to the dielectrophoretic trapping of DNA reported by Chou et al.[4]

The applied time-dependent voltage $U(t)$ leads to an inhomogeneous electric field $\vec{E}\sin(\omega t)$ in the structured region, with a field strength $\vec{E}$ proportional to U_{ac} and with the spatial periodicity of the structure. For polarizable molecules with polarizability $\alpha = \alpha(\omega)$, this field creates a dielectrophoretic potential landscape given by

$$W = -(1/2)\alpha\vec{E}^2 \qquad (1)$$

In this description, adsorption effects are neglected so that the polarizability α is real-valued. For $\alpha > 0$, the molecule is driven toward the regions of strongest field amplitudes, which represent the minimums of W (positive dielectrophoresis), while for $\alpha < 0$, regions with smallest field amplitudes form the potential minima (negative dielectrophoresis). As illustrated in Figure 2b, the

potential (1) with $\alpha > 0$ has deep minimums within the gaps in the regions close to the post walls where the DNA is observed to be trapped, indicating that the trapping is due to positive dielectrophoresis. Our detailed experimental studies yield that such dielectrophoretic trapping occurs for T2 (164 kbp) and also for λ (48.5 kbp) DNA over a frequency range of $\sim$30−200 Hz of the ac voltage. This compares well with the frequency range of 50 Hz−1 kHz for which trapping has been observed by Chou et al.[4] despite the different post array structure and buffer conditions. Moreover, for the frequencies and conditions studied here, no back-and-forth motion of the DNA molecules due to electrophoretic effects of the ac field could be observed. Therefore, the averaged dielectrophoretic potential (1) constitutes an appropriate model for the impact of the ac voltages $U(t)$ on the DNA.

The idea of exploiting dielectrophoresis for the separation of DNA is based on the following two observations. First, the depth of the potential (1) depends on the polarizability of the DNA, and second, the polarizability of (short) DNA fragments (up to $\sim$5kbp) is known to increase with their lengths.[17] Using a simplified one-dimensional model, Ajdari and Prost[38] predicted size separation of DNA with length-dependent polarizabilities due to different average migration velocities, when an appropriate static force is applied in addition to the dielectrophoretic traps. Similarly, Chou et al.[4] suggested to selectively trap one sort of DNA while removing another one. We demonstrate the feasibility of this separation principle with the following experiments.

DNA Separation by Electrodeless Dielectrophoresis. In order to impose an additional constant force on the DNA in the microstructure, a static voltage component U_{dc} is superimposed onto the oscillating signal $U(t)$. For the separation of two different DNA lengths, an optimal choice of U_{dc} and of the ac amplitude U_{ac} should permanently trap one DNA species whereas the other one can migrate along the microchannel. This requires precise knowledge of polarizabilities and electrophoretic mobilities of the DNA molecules for the given experimental conditions. Such information, however, is usually not accessible before separation, so that it is very difficult to predict the appropriate values of U_{dc} and U_{ac} for an efficient separation experiment.

For this reason, we use the following separation protocol. After injection of the DNA sample into the structured channel, a fixed dc component U_{dc} is applied, and different U_{ac} values are probed by increasing U_{ac} from U_{start} to U_{end} in discrete steps of size U_{inc} and duration τ_{inc}. When U_{end} is reached, U_{ac} is set to the maximum value U_{max} and the static-voltage component U_{dc} is switched off to create steady-state trapping conditions for electropherogram recording (see also Materials and Methods).

We perform such separation experiments with two different DNA samples: (a) a mixture of linear DNA fragments, composed of λ- and T2-DNA at concentrations 41 and 6.1 pM, respectively; (b) a sample of ccc plasmid DNA, containing a 7-kbp plasmid and its 14-kbp dimer in a concentration ratio of 9:1. The measured steady-state electropherograms are shown in Figure 3, demonstrating the successful separation of both samples with baseline resolution. The different DNA fragments in the samples are attributed to the peaks of the electropherograms by comparison with control experiments performed for the individual λ- and T2-DNA and by spiking experiments for the 7- and 14-kbp ccc plasmids. Moreover, the λ- and T2-DNA can be distinctively

(41) http://www.nag.co.uk/.
(42) Seiler, K.; Fan, Z. H.; Fluri, K.; Harrison, D. J. *Anal. Chem.* **1994**, *66*, 3485−91.
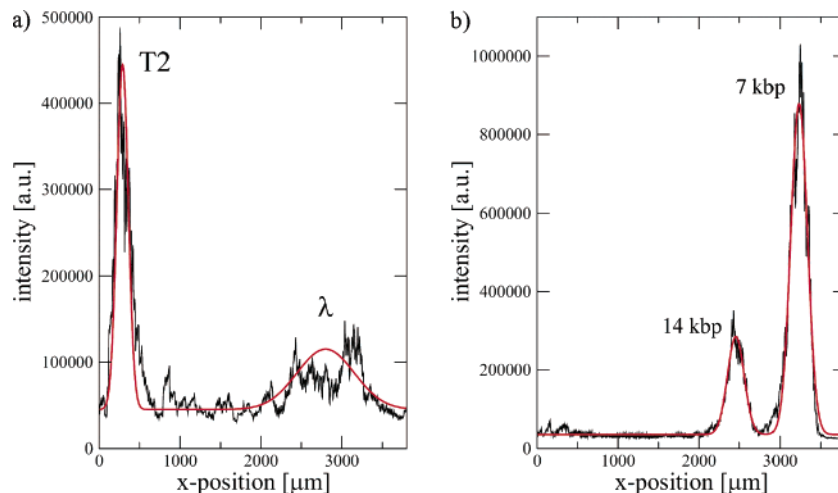
Figure 3. Steady-state electropherograms after application of the separation protocol for a) a λ- and T2-DNA sample (static voltage, $U_{dc} = 12$ V; voltage ramp, $U_{start} = 150$ V, $U_{inc} = 0.6$ V, $\tau_{inc} = 3$ s, $U_{end} = 189$ V, $\omega = 60$ Hz), and (b) a 7-kbp ccc-plasmid DNA and its 14-kbp dimer (static voltage, $U_{dc} = 12$ V; voltage ramp, $U_{start} = 198$ V, $U_{inc} = 6$ V, $\tau_{inc} = 30$ s, $U_{end} = 240$ V, $\omega = 60$ Hz). For both samples, the two DNA species have been trapped at different locations in the separation channel and thus could be separated with baseline resolution. The peaks of the shown "steady-state electropherograms" are fitted by Gaussian curves in order to guide the eye and for calculating the resolution (see eq 2).

identified during the migration process due to significantly different fluorescence intensities. From the results in Figure 3, we see that in both experiments the longer DNA is trapped first in the separation channel, i.e., at smaller values of U_{ac}, indicating that the DNA polarizability increases with the DNA length. The relation between DNA length and polarizability will be studied in greater detail below (see DNA Polarizabilities).

In order to quantify the efficiency of the dielectrophoretic separation method, we calculate the resolution R as usual for zone separations according to[43]

$$R = (x_2 - x_1)/[2(\sigma_1 + \sigma_2)] \qquad (2)$$

Here, x_1 and x_2 are the positions of the centers of Gaussian curves fitted to the measured peaks in Figure 3 and σ_1 and σ_2 are their width (standard deviations); the subscripts 1 and 2 refer to the two DNA species for which the separation resolution is determined. For the separation of λ- and T2-DNA, we find $R = 2.95$; this resolution is achieved within a separation time of 200 s (see the driving parameters in Figure 3a). The plasmid sample with 7- and 14-kbp plasmid DNA is separated with resolution $R = 1.93$ within 240 s (see Figure 3b). In both cases, the fluorescence detection takes ~6 min, so that the complete experiments can be performed in ~10 min.

Quantitative Description of the DNA Migration. For the analysis of the DNA migration, we do not consider the U_{ac} ramp used for the separation experiments, but focus on constant amplitudes U_{ac} of the ac voltage $U(t)$. As described above, the ac voltage creates a dielectrophoretic potential (1) for the DNA molecules with traps in the gaps between two posts close to the post walls (see Figure 2). The DNA can escape from such a trap only due to the ambient thermal noise. For large U_{ac}, the dielectrophoretic potential barrier that has to be surmounted for escaping from a trap is much larger than the thermal energy $k_B T$,

(43) Giddings, J. C. *Unified separation science*; John Wiley Sons: New York, 1991.

so that such an escape process is a very rare event, in accordance with our observations of "permanent" DNA trapping described in Figure 2. When the dc voltage U_{dc} is applied in addition to $U(t)$, the induced electrokinetic force along the channel axis effectively tilts the dielectrophoretic potential. Note that for our experimental conditions this electrokinetic force is mainly of electrophoretic character, as the electroosmotic flow is effectively reduced by a PEG-silane coating[39] and the POP-6 polymer additive. As long as the dielectrophoretic trapping force is larger than the electrophoretic force, the DNA molecules are still trapped deterministically by the dielectrophoretic potential and can escape only due to the thermal noise. Once escaped from a trap, the DNA is electrophoretically driven along the channel until it is trapped by the next trap on its way. For appropriate (not too large) U_{ac} values, the barrier heights of the (tilted) dielectrophoretic potential are comparable to $k_B T$, so that escapes from the trap are sufficiently fast to yield average migration velocities of the DNA in the micrometer per second range. According to (1), the depth of the dielectrophoretic potential depends on the DNA polarizability, and so does the mean escape time from the trap, leading to different migration velocities for different DNA molecules. In contrast, if the dielectrophoretic trapping force is smaller than the electrophoretic force, (i.e., small U_{ac} or large U_{dc}), the traps completely disappear and the migration velocity of the DNA is determined by its length-independent electrophoretic mobility.

From the video sequences recorded, we observe that the migration of a DNA molecule along the channel (x direction) from trap to trap basically proceeds within a sequence of gaps at identical y position. Therefore, we can neglect its (predominantly diffusive) motion in the direction perpendicular to the channel axis and adopt the approximate picture of the DNA moving along the x direction in a one-dimensional, tilted periodic potential with deep and narrow potential minimums that represent the dielectrophoretic traps. Moreover, from an estimation of the curvatures Ω^2 of the dielectrophoretic potential (1) in the direction of motion (x direction), we find for the "deformation energy" $\Omega^2 l^2$ at the length scale of the persistence length $l \approx 50$ nm of the DNA that

$\Omega^2 l^2 \ll k_B T$ (except for very small regions at the corners of the posts (see Figure 2b). Hence, the DNA molecules remain in a quasi-stationary globular configuration throughout the complete migration process. The escape time τ of a DNA molecule out of the dielectrophoretic trap due to thermal activation is then given by the inverse Kramers rate,[44,45]

$$\tau \propto \exp\left(\frac{\Delta W - \Delta W_{dc}}{k_B T}\right) \qquad (3)$$

where ΔW denotes the dielectrophoretic potential barrier reduced by the electrophoretic energy drop ΔW_{dc} due to the static voltage U_{dc}.

Within this simplified picture, the DNA motion in the microfluidic channel is approximately described by the one-dimensional model of Ajdari and Prost[38] for a pointlike polarizable particle moving in a static tilted periodic potential. Accordingly, the average migration velocity v of a DNA molecule in the microchannel for constant U_{ac} and U_{dc} reads[38]

$$v = L/(\tau + t_0) \qquad (4)$$

where L is the period of the structure in x direction (see Figure 1), t_0 the time for migrating along the channel axis from a gap between two posts to the next (at identical y position) without dielectrophoretic traps (i.e., at $U_{ac} = 0$V), and τ the mean escape time from a trap according to (3).

The dielectrophoretic potential barrier ΔW in (3) can be quantified as follows. From eq 1, we obtain $\Delta W = (1/2) \alpha(E_{gap}^2 - E_{mid}^2) = (1/2) \alpha E_{gap}^2 (1 - E_{mid}^2/E_{gap}^2)$. The mean field strength E_{gap} in a gap represents an approximation of the average field the trapped DNA actually feels (i.e., the field strength averaged over the typical extension of a DNA molecule in the trap). The field strength E_{mid} in the middle between two rows of posts is practically constant over the entire channel cross section. Since the electric field fulfills the condition $\nabla \cdot \vec{E} = 0$, these field strengths are related according to $E_{mid}/E_{gap} = Y_{gap}/Y_{mid}$, where Y_{gap} and Y_{mid} are the widths (in y direction) of the fluid-accessible part of channel 2 (see Figure 1) at a row of posts and in the middle between two rows of posts, respectively. For our microstructure we have $Y_{gap} = 23$ μm and $Y_{mid} = 100$ μm, so that $E_{mid}/E_{gap} = 0.23$. Moreover, E_{gap} is proportional to the amplitude U_{ac} of the ac voltage with a proportionality factor that can be calculated as described in Materials and Methods, so that we obtain in good approximation

$$\Delta W = 22900 \alpha U_{ac}^2 \text{m}^{-2} \qquad (5)$$

DNA Polarizabilities. The insight into the DNA motion along the microchannel gained from its theoretical description in the previous section offers a new method to quantitatively determine the DNA polarizability. For not too small U_{ac}, the dielectrophoretic traps are deep enough (compared to $k_B T$) for the rate description (3) to be valid. Then, the mean escape time τ out of the dielectrophoretic traps is expected to depend linearly on U_{ac}^2 (see eq 5), with logarithmic corrections of the form $\ln U_{ac}^2$ that

stem from the prefactor in (3), since this prefactor also depends on (derivatives of) the potential[44,45] and thus on U_{ac}^2. From the linear contribution in the U_{ac}^2 dependence, one can calculate the polarizability α according to (5). Therefore, the experimental challenge consists in measuring τ for varying U_{ac}. This is done by observing the DNA migration along the microchannel for a fixed value of U_{dc} and different ac amplitudes U_{ac}. We performed such experiments at $U_{dc} = 12$ V for linear DNA fragments of four different lengths: 6, 12, 48.5 (λ-DNA), and 164 kbp (T2-DNA). The results are summarized in Figure 4.

In Figure 4a, the average migration velocities determined from the recorded video sequences are shown. At low ac amplitudes, the different DNA species exhibit similar migration velocities, because the effect of the dielectrophoretic potential is negligible and the size-independent electrophoretic motion[46] dominates. At larger U_{ac} values ($U_{ac} \geq 100$ V), the retarding effect of the dielectrophoretic traps becomes significant, and considerably different average migration velocities are measured for the different DNA lengths, in accordance with the theoretical prediction by Ajdari and Prost.[38] At those values of U_{ac}, at which the velocity curves in Figure 4a end, permanent trapping of the respective DNA species is observed (within our observation time). We see that longer DNA fragments move slower and that permanent trapping occurs at smaller ac amplitudes U_{ac} confirming the observed migration order in our separation experiments (see Figure 3).

From the average migration velocities of Figure 4a, the mean escape times are obtained using eq 4 after determining the free traveling time t_0 (which only depends on U_{dc} but not on U_{ac}) between two successive rows of posts from the recorded video sequences. For $U_{dc} = 12$ V we find $t_0 = (1.0 \pm 0.1)$ s per spatial period $L = 21.1$ μm of the post array for all four DNA lengths, concluding that t_0 is independent of the DNA length. The corresponding size-independent free solution DNA mobility $\mu_0 = (3.5 \pm 0.4) \times 10^{-8}$ m^2/V·s is in very good agreement with literature values[47] ranging from 3.0×10^{-8} to 4.5×10^{-8} m^2/V·s.

Figure 4b demonstrates the dependence of the mean escape time τ on the applied ac amplitude U_{ac}. The expected dominating dependence of $\ln\tau$ on U_{ac}^2 (see eqs 3 and 5) for larger voltages U_{ac} (i.e., sufficiently deep traps) is confirmed. The different slopes of the logarithmic escape times for different DNA species indicate that the polarizability α depends on the length of the DNA molecule. By fitting the measured data (taking into account the above-mentioned logarithmic corrections) in the range of validity of the rate law (3), the polarizabilities for the DNA fragments are calculated from the slope according to (5). The results are summarized in Table 1. They are comparable to the DNA polarizabilities reported in the literature (see Table 2), although a direct comparison seems questionable in view of the various measurement methods, frequency ranges, and buffer systems used. Moreover, for our method, the necessary DNA staining alters the actual charge on the DNA molecule and thus may also change the polarizability of the DNA.

In Table 1, trapping forces are also listed, which we calculate from the measured polarizabilities for an ac voltage $U_{ac} = 140$ V. Since this value is applied over a distance of ~7 mm in our device,

(44) Hänggi, P.; Talkner, P.; Borkovec, M. *Rev. Mod. Phys.* **1990**, *62*, 251−341.
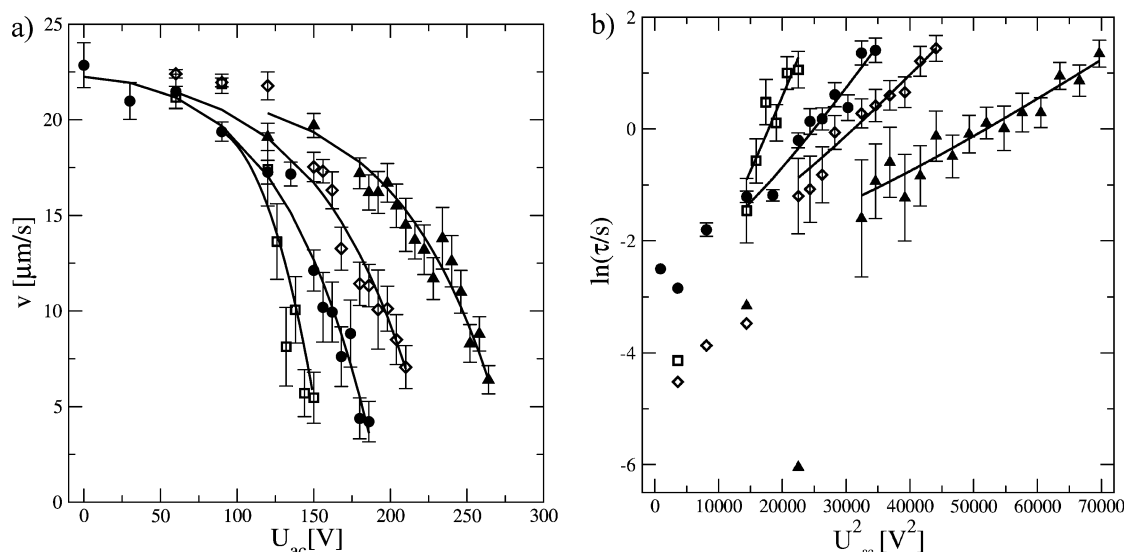(45) Park, P. J.; Sung, W. *J. Chem. Phys.* **1999**, *111*, 5259−66.

(46) Viovy, J.-L. *Rev. Mod. Phys.* **2000**, *72*, 813−72.
(47) Stellwagen, N. C.; Gelfi, C.; Righetti, P. G. *Biopolymers* **1997**, *42*, 687−703.

Figure 4. (a) Average velocity v versus applied ac amplitude for 6 kbp (▲), 12 (◇), 48.5 (●), and 164 kbp (□) DNA at frequency $\omega = 60$ Hz and for $U_{dc} = 12$ V. The velocities are determined from recorded video sequences by averaging over ∼30 individual DNA molecules at each value of U_{ac} and for each DNA species. The longer DNA fragments are clearly retarded in comparison with the shortest 6-kbp DNA. At the "end points" of the velocity curves at large U_{ac} values, the migration velocity becomes immeasurably small, because the DNA is trapped permanently (within our observation time). The solid lines represent data fits as a guide to the eye. (b) Mean escape times τ are plotted versus the square of the applied ac voltage U_{ac} (symbols as in a) in a logarithmic scale. The mean escape times were determined according to (4) from the average velocities v in (a) and the free traveling time $t_0 = (1.0 \pm 0.1)$ s (see also main text). The expected basically linear dependence is confirmed for larger U_{ac}, where the rate description (3) becomes valid. Note that for such U_{ac} amplitudes the average velocities in (a) are significantly smaller than the free traveling velocity. The solid lines represent data fits within those U_{ac} regions.

Table 1. DNA Polarizabilities α for Varying DNA Lengths, Determined by Dielectrophoretic Trapping of DNA[a].

DNA (kbp)	α (Fm²)	trapping force (fN)
6	$(1.5 \pm 0.1) \times 10^{-29}$	3.1
12	$(2.5 \pm 0.2) \times 10^{-29}$	5.0
48.5 (λ-DNA)	$(3.3 \pm 0.3) \times 10^{-29}$	6.6
164 (T2-DNA)	$(5.8 \pm 0.5) \times 10^{-29}$	11.8

[a] The given errors result from the statistical uncertainties in the mean escape time τ. Also shown are the estimated trapping forces for $U_{ac} = 140$ V.

it is comparable to the voltage 200 V that Chou et al.[4] applied at their device of length 1 cm. The maximum trapping forces of 1.6 fN for 4.36-kbp DNA (comparable in length to our 6-kbp DNA) and of 5.8 fN for 39.9 kbp DNA (comparable to our λ-DNA) reported by Chou et al.[4] are in good agreement with our estimations of 3.1 and 6.6 fN, respectively. This is surprising in view of the differences in the buffer systems, DNA lengths, and frequency ranges.

For the long DNA fragments studied here, we may expect that dependencies on the DNA length (which is proportional to the number N of base pairs) can be described by scaling laws. Therefore, assuming that for the DNA polarizability α a relation $\alpha \sim N^\gamma$ holds, we obtain $\gamma = 0.4 \pm 0.1$ for the scaling exponent (see Figure 5). This value is considerable smaller than the previously published exponents. For example, Stellwagen[18] reported a quadratic relation between α and N for DNA lengths below ∼300 bp. Elias and Eden[19] found $\gamma = 3$ in a range up to ∼120 bp lengths passing into a linear relation ($\gamma = 1$) above ∼300 bp up to 5 kbp. Moreover, a cubic dependence is evidenced by

Porschke et al.[17] for DNA lengths below ∼400 bp, whereas for longer DNA, they observed saturation of the polarizability. Note, however, that the DNA fragments between 6 and 164 kbp studied here are considerably larger than those in the previous studies.[17−19]

Finally, we remark that the deduced value for γ is close to the theoretical Flory exponent of 0.6 for linear chainlike polymers in three dimensions.[46] This suggests that polarization of long DNA fragments is driven by charge displacement along the DNA strand and results in an effective polarization that linearly scales with the end-to-end distance of the DNA molecule, as previously anticipated by Bowers and Prud'homme.[48] However, in view of the differing findings in the literature[17−19] (although for shorter DNA lengths) and of our limited amount of data (four DNA lengths), a more detailed analysis employing a broader range of DNA fragment sizes should be accomplished in the future.

CONCLUSIONS

In this work, the manipulation of long DNA fragments by electrodeless dielectrophoresis in a microstructured array of posts combined with electrophoretic forcing has been studied in two respects: sorting of DNA according to length and measurement of DNA polarizabilities.

A separation technique for DNA molecules with length-dependent polarizabilities based on the combination of free-flow electrophoresis with dielectrophoretic trapping had been suggested theoretically 15 years ago.[38] However, experimental proof has not yet been reported in the literature, probably due to the delicate balance between dielectrophoretic, electrophoretic, and thermal forces ("noise") necessary for successful separation. Here, we showed that this difficulty can be handled by systematic

(48) Bowers, J. S.; Prud'homme, R. K. *J. Chem. Phys.* **1992**, *96*, 7135−43.

Table 2. DNA Polarizabilities for Various DNA Lengths and Buffer Conditions As Reported in the Literature[a]

reference	DNA (kbp)	α (Fm^2)	method	buffer system
Stellwagen[18]	4.4	5.5×10^{-31}	transient electric birefringence (TEB)[b]	Tris (0.2 mM, pH 8)
Elias & Eden[19]	5	2.3×10^{-30}	TEB[b]	sodium phosphate (1 mM Na, pH 7.2)
Hanss & Bernengo[21]	8	3.2×10^{-28}	conductivity dispersion[c]	1 mM NaCl
	16	3×10^{-27}		
Bakewell et al.[16]	12 (plasmid)	7.88×10^{-30}	time domain reflectometry[d]	dd H$_2$O
Rau & Bloomfield[20]	40 (T7 DNA)	1.3×10^{-28}	TEB[c]	sodium phosphate (0.5 mM Na, pH 6.9)

[a] Also shown are the experimental methods from which the polarizabilities are obtained. The list is restricted to DNA lengths that are comparable to our DNA lengths. [b] Frequency >1kHz. [c] Frequency <1kHz. [d] Frequency 137 kHz.
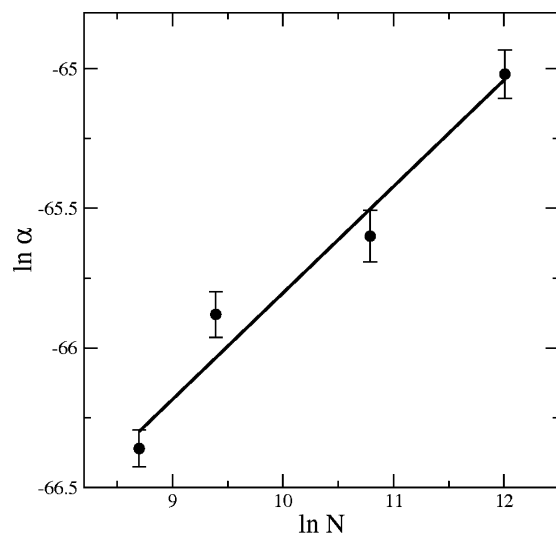

Figure 5. Dependence of the DNA polarizability on the number of base pairs. ln α is plotted against ln N revealing an exponent $\gamma = 0.4 \pm 0.1$.

variation of the dielectrophoretic force strength during the electrophoretic migration of the DNA in the microstructure, demonstrating successful separation of linear DNA (λ (48.5-kbp) and T2 (164-kbp) DNA) and ccc plasmids (7- and 14-kbp). The separation times of the order of a few minutes and the achieved (baseline) resolutions compare very well to other microfluidic separation methods proposed in the literature for comparable DNA sizes, such as magnetic bead arrays[28] or entropic traps.[32] The separation experiments present a proof of the concept of DNA sorting by dielectrophoretic trapping and, as such, leave room for optimization (e.g., of the trap geometry or the electric driving parameters). In particular, we expect that tuning the protocol used for variation of the dielectrophoretic trapping forces during separation (the U_{ac} ramp) in order to further improve the resolution and the addressable DNA fragment range is promising.

A detailed analysis of the DNA migration in the separation experiments revealed that the escape times out of the dielectrophoretic traps differ with the length of the DNA due to the length-dependent polarizabilities. Therefore, separation indeed occurs according to the mechanism proposed by Ajdari and Prost.[38]

Moreover, it turned out that the DNA polarizabilities can be determined quantitatively from the mean escape times of the thermally activated escape processes. We applied this new measurement method to four linear DNA fragments in a size range from 7 to 164 kbp and observed an increase of the polarizability with the DNA length. This length dependence, however, is quite weak; we found evidence that it scales with the end-to-end distance of the DNA molecule. The reason that nevertheless efficient separation is possible lies in the escape processes from the traps, in which polarizability differences are amplified exponentially (cf. the Kramers mean escape time (3) and the dielectrophoretic potential (1)).

The simplicity of the newly developed measurement method for the DNA polarizability may open the way to systematic experimental studies including its dependence on the ac driving frequency, buffer conditions, DNA conformation, etc. Furthermore, both principles—dielectrophoretic separation and polarizability measurement—are not restricted to DNA (of a certain length range), but may be applied to any polarizable migrant, for instance, other biomolecules such as proteins. In particular, the dependence of the polarizability on topological conformations of DNA molecules could be envisaged. This would have direct impact on the quality control of plasmid samples for biotechnological applications like gene therapy and DNA vaccination.